

First-Principles Study of the Bonding and Mechanical Properties of Metallic Grain Boundaries

M. Kohyama¹, S. Tanaka¹, R.Z. Wang², Y. Shiihara³, S. Saitou⁴, T. Tamura⁵ and S. Ishibashi⁵

¹Research Institute for Ubiquitous Energy Devices, National Institute of Advanced Industrial Science and Technology, Japan

²College of Materials Science and Engineering, Beijing University of Technology, China

³Institute of Industrial Science, The University of Tokyo, Japan

⁴National Institute for Materials Science, Japan

⁵Research Institute for Computational Sciences, National Institute of Advanced Industrial Science and Technology, Japan

Grain boundaries (GBs) have serious effects on the mechanical properties of metals, and the understanding of primary behavior of GBs under various stresses is crucial. First-principles tensile or shear tests of GBs are quite effective to understand such behavior of GBs, and the energy-density and stress-density schemes are effective tools to analyze both the electronic and mechanical properties directly. In this paper, we examine the bonding and mechanical properties of GBs in Al and Cu by using these tools. First, we examine the stability and bonding of tilt and twist GBs as well as stacking faults and twins in Al and Cu. We have observed remarkable effects of electronic structure of each metal species. Second, we apply the local energy-density and stress-density schemes to GBs. Third, we perform first-principles tensile tests of Al tilt and twist GBs, where we examine the effects of segregated Si and Mg impurities. We have found opposite effects of Si and Mg, which are consistent with recent experiments of Al samples.

Keywords: *first-principles calculation, grain boundary, impurity segregation, electronic structure, tensile strength.*

1. Introduction

Grain boundaries (GBs) have serious effects on the mechanical properties of metals as barriers of dislocation transmission or as sources or sinks of dislocations. This feature is greatly enhanced in nano- or sub-micron grained metals formed by severe plastic deformation [1, 2]. Thus the understanding of primary behavior of GBs under various stresses is crucial. First-principles tensile or shear tests of GBs [3] are quite effective to understand such behavior of GBs via the behavior of atoms and electrons. As a tool to analyze both the electronic and mechanical properties more directly, we have developed the energy-density and stress-density schemes [4] in our original *ab initio* code QMAS (Quantum Materials Simulator) [5]. In this paper, we examine the bonding and mechanical properties of GBs in typical *fcc* metals, Al and Cu by using these tools. First, we examine the stability and bonding of tilt and twist GBs [6] as well as stacking faults (SFs) and twins in Al and Cu. Second, we apply the local energy-density and stress-density schemes to GBs. Third, we perform first-principles tensile tests of Al tilt and twist GBs in order to examine the ideal strength and features of deformation and failure. Then we examine the effects of Si and Mg impurities segregated at Al GBs in the tensile tests, which are compared with recent experiments of Al poly-crystalline samples formed by severe plastic deformation [7].

2. Theoretical Method

We use the projector-augmented wave (PAW) method [8] based on the density-functional theory (DFT) within the generalized gradient approximation (GGA) [9] via our original program code

QMAS. The PAW method is the most improved scheme within the pseudo-potential framework with both excellent accuracy and efficiency. Realistic oscillating behavior of valence-wave functions near nuclei is accurately reproduced by the replacement of the expansion with pseudo partial waves by the expansion with all-electron partial waves via the projection of pseudo-wave functions, differently from the conventional pseudo-potential schemes. In QMAS, the electronic ground state is obtained iteratively by the block-Davidson scheme [10, 11] coupled with the efficient Kerker-Pulay charge-mixing scheme [12, 13] using the technique of MPI parallelization [14]. The plane-wave cut-off energy is 40Ry for Al and Cu, and the k -point sampling is performed by the Monkhorst-Pack scheme [15]. The self-consistent convergence criteria is 1.0×10^{-5} e/a.u.³ For bulk *fcc* crystals, we obtained the lattice constants of 4.03Å for Al and 3.63Å for Cu, which are in good agreement with experiments.

We deal with typical coincidence-site-lattice (CSL) GBs [16], the $\{221\}\Sigma=9$ tilt and $\{001\}\Sigma=5$ twist GBs in Al and Cu, which have two-dimensional periodic configurations. The $\{221\}\Sigma=9$ tilt GB in *fcc* metals is constructed by rotating one grain with 38.94° along the common [110] axis and setting (2,-2,1) as a GB plane. The $\{001\}\Sigma=5$ twist GB in *fcc* metals is constructed by rotating one grain with 36.87° along the common [001] axis and setting (001) as a GB plane. We deal with the glide and mirror models for the $\{221\}\Sigma=9$ tilt GB [17] via 42-atom and 36-atom supercells, and we use 50-atom supercells for the $\{001\}\Sigma=5$ twist GB. We also deal with SFs using supercells of 11 $\{111\}$ atomic layers containing one interface consisting of *hcp*-like stacking, and we deal with twins using supercells of 20 $\{111\}$ atomic layers containing two interfaces consisting of *hcp*-like stacking. For each supercell, we use enough dense k -point meshes similar to the bulk crystal calculation. This point is crucial to obtain accurate energies especially for SFs and twins. In the relaxation of GB models according to Hellman-Feynman forces, the force convergence criteria is set as 1.0×10^{-4} Hartree (Ht)/a.u. In this way, we can obtain the energy and atomic and electronic structures of stable configurations of GBs, SFs and twins in Al and Cu.

3. Energies and Interfacial Bonding of Grain Boundaries and Stacking Faults in Al and Cu

Calculated results of the energies and structures of GBs, SFs and twins are listed in Table 1. The energy value is the increase against the bulk crystal of the same number of atoms. The GB excess volume is the volume expansion against the stacking of bulk layers. The SF and twin energies are in good agreement with experiments [18] and other theoretical results [19, 20]. The energies of Al are larger than those of Cu. This can be explained by the covalent nature or sensitivity for distant structure in Al. The SF and twin energies can be approximated by the energy difference between *fcc* and *hcp* structures. For Cu with a closed-shell *d* band and *s* electrons, the energy of crystal or defect structures can be described by rather short-range inter-atomic interactions, due to rapid decrease of *d-d* orbital interactions, which results in a rather smaller *hcp-fcc* energy difference. On the other hand, for Al with *sp* electrons, the energy of crystal or defect structures is described by rather long-range inter-atomic interactions [21], due to slowly decreasing *s-s*, *s-p* and *p-p* orbital interactions and easy charge redistribution by higher valence-electron density, resulting in larger SF and twin energies.

For GBs in each metal species, the $\Sigma=5$ twist GB is the most stable, and the glide model is more stable than the mirror one for the $\Sigma=9$ GB, in accordance with the degree of structural distortions. Thus the GB energy has the correlation with the excess volume via the structural distortions. Our results of GBs are consistent with other *ab initio* results [22-24]. The mirror model of the $\Sigma=9$ GB is constructed by bulk layers without removing atoms, differently from that in [24]. It is quite interesting that the GB energy for Cu is generally larger than Al, differently from the SF and twin energies. Similarly the surface energies of Cu [25] are larger than those of Al in spite of similar cohesive energies (Cu: 3.49eV/atom, Al: 3.39eV/atom). The vacancy formation energy in Cu (1.30 eV) is also much larger than that in Al (0.68 eV) experimentally. This leads to a hypothesis that the covalent nature of Al may generally reduce defect energies in Al, namely stabilize defective

structures via electronic and atomic behavior of reconstruction as observed in *ab initio* results of Al surfaces [26], point defects [27] and greatly sheared Al [19].

Table 1. Calculated results of the $\Sigma=5$ twist GBs, the glide and mirror models of the $\Sigma=9$ tilt GBs, SFs and twins in Al and Cu. The SF-energy values in parentheses are the experimental ones [18].

	$\Sigma=5$ Twist	$\Sigma=9$ Glide	$\Sigma=9$ Mirror	SF	Twin
Energy (mJ/m ²)	Al: 351 Cu: 698	Al: 453 Cu: 755	Al: 656 Cu: 1152	Al: 134 (166) Cu: 42 (45)	Al: 62 Cu: 27
Excess Volume (nm)	Al: 0.034 Cu: 0.038	Al: 0.054 Cu: 0.045	Al: 0.064 Cu: 0.056		
Bond-Length Change	Al: -7.5%~5.2% Cu: -7.0%~4.6%	Al: -6.4%~4.8% Cu: -7.0%~5.6%	Al: -10.5%~11.3% Cu: -10.9%~10.5%		

We can see such covalent nature of Al in Figs. 1 and 2, revealing the electronic behavior of interfacial bond-reconstruction at Al GBs. The features of valence charge distribution at the interfaces of the Al GBs are quite different from those in Al bulk regions and in the Cu GBs. In both the tilt and twist GBs in Al, there are remarkable charge accumulations at the reconstructed bonds between less-coordinated interfacial atoms. In contrast, there is no remarkable charge redistribution in the same GBs in Cu, where only spherical *d*-electron distributions centered on each atom are seen.

In this way, the covalent nature of Al should stabilize defective structures via electronic and atomic behavior of reconstruction, namely via charge accumulation or directional-bond formation at less-coordinated or distorted atoms, which should lower the energies of GBs, surfaces and point defects in Al, compared with those in Cu. However, note that the covalent nature of Al leads to larger SF and twin energies than those of Cu, oppositely due to the sensitivity for distant structures.

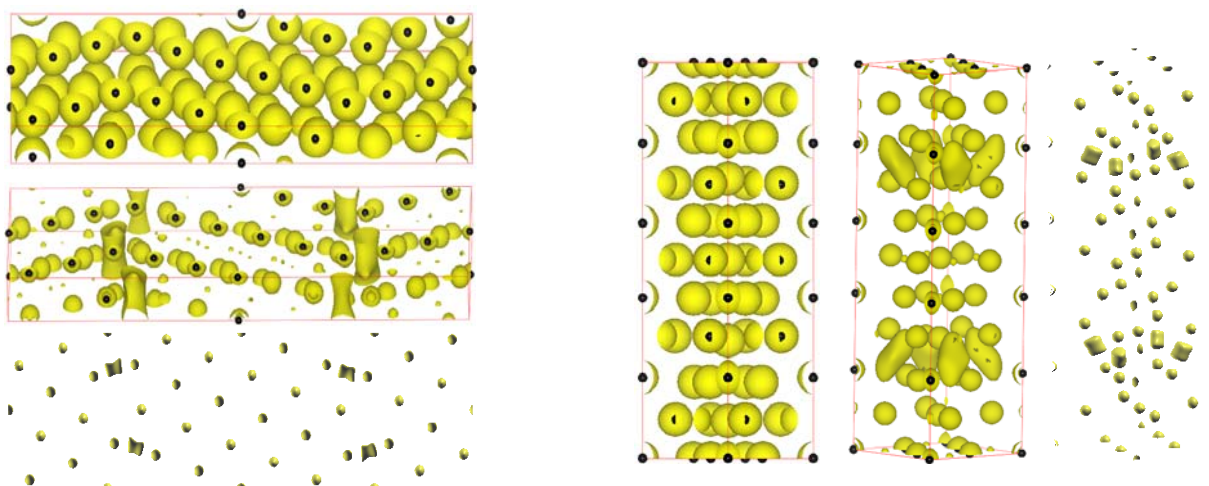


Figure 1 (Left). Charge-density iso-surfaces in the supercells of the $\Sigma=9$ tilt GB (glide model) in Cu (top panel) and Al (middle and bottom panels). There are two interfaces in the cell. The iso-surface charge values in these panels are 0.051 (top), 0.017 (middle) and 0.034 (bottom). The bottom panel shows clear charge accumulation at the interfacial reconstructed bonds.

Figure 2 (Right). Charge-density iso-surfaces in the supercells of the $\Sigma=5$ twist GB in Cu (left panel) and Al (central and right panels). There are two interfaces in the cell. The iso-surface charge values in these panels are 0.051 (left), 0.017 (central) and 0.034 (right). The right panel shows clear charge accumulation at the interfacial reconstructed bonds.

4. Energy Density and Stress Density Analysis

In the first-principles methods using a plane-wave basis, the total energy and stress tensor [28] are obtained as integrals inside the supercell. As shown in Eq. 1, it is possible to define the energy density and stress density as distribution functions $e_{tot}(\vec{r})$ and $\tau_{\alpha\beta}(\vec{r})$ periodic in each cell, of which the integrations throughout the cell volume Ω correspond to usual quantities of the total energy and stress tensor. The energy density and stress density can be used to analyze local distributions of energy and stress at defects, surfaces or interfaces in the supercell. Practical schemes to perform such calculations within the DFT pseudo-potential methods were proposed in [29, 30], while there have been only few applications due to complicated programming and a serious problem of gauge dependency [29, 30].

$$E_{tot} = \int_{\Omega} e_{tot}(\vec{r}) d\vec{r}, \quad \sigma_{\alpha\beta} = \frac{1}{\Omega} \int_{\Omega} \tau_{\alpha\beta}(\vec{r}) d\vec{r} \quad (1)$$

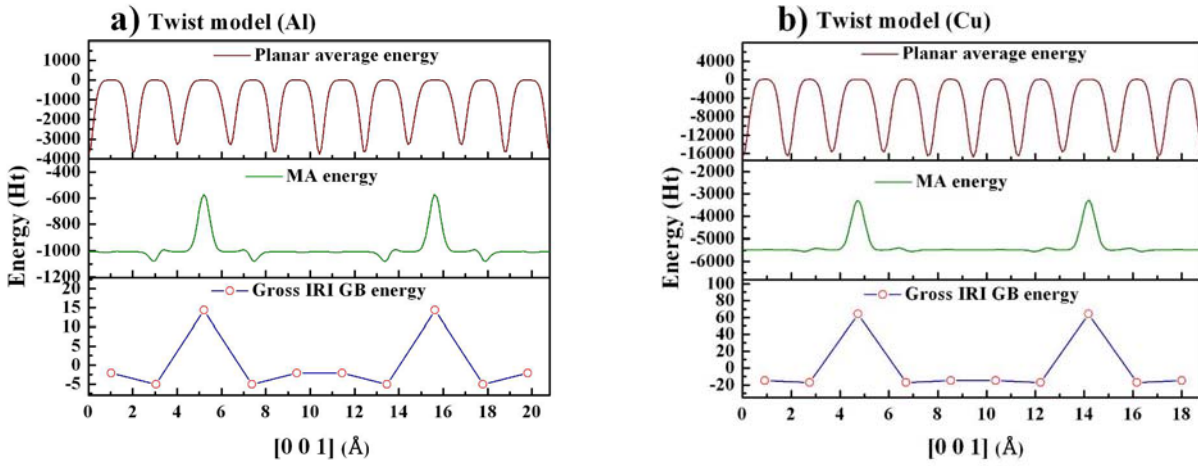


Figure 3. Energy-density analysis of the $\Sigma=5$ twist GBs in Al (a) and Cu (b). Averaged energy density values on each $\{001\}$ plane are plotted along the $\langle 001 \rangle$ axis. Raw data (top), *macroscopic averaging* data (middle) and inter-layer integrated data (bottom) are plotted.

Recently, we have developed the program for the energy-density and stress-density schemes within the PAW method in QMAS [4], which should be useful to analyze the effects of local structural disorder on the interfacial bonding and mechanical properties of GBs and SFs. Figure 3 shows the application of the energy-density scheme to the $\Sigma=5$ twist GBs in Al and Cu, indicating clearly the energy increase at the interfaces in the supercell. However, it should be noted that the energy or stress distribution functions themselves *cannot* be regarded as *unique* functions, because these depend on the selection of the forms of kinetic energy- or stress-density functions, for example. This is called as gauge-dependent problem [4]. It is necessary to make some operation to remove such effects. Historically, two methods have been adopted as shown in Fig. 3 [29, 30]. One is to perform *macroscopic averaging* as cyclic integration of one-dimensional averaged profile, and the other is to integrate the functions inside each *local region* such as each atomic layer to obtain local energy or stress values instead of density values. However, these two methods have some faults and there have been no rigorous methods to remove the gauge-dependent problem completely. Recently, we have developed a new effective scheme [4], where the *local region* for the integration is defined so as to make the difference between the symmetric and asymmetric forms of the kinetic energy- or stress-density functions zero in integrating the functions in such a region. By this new method, we can make effective analyses of the effects of GBs and SFs on the bonding and mechanical properties in the near future.

5. First-principles Tensile Tests of Al Grain Boundaries

In the first-principles tensile test [3, 31], the supercell of a GB is gradually stretched in the direction normal to the GB plane. The atomic positions are linearly changed for the discrete supercell-length change, and all the atoms are relaxed according to the atomic forces. This cycle is iterated until the failure occurs. We can observe the behaviour of atoms and valence electrons under tensile stress, and we obtain the energy-strain and stress-strain curves, providing ideal tensile strength of a GB, namely upper limit of tensile strength without effects of temperature or defects. This type of calculations has been widely applied to GBs in various materials and various metal/ceramic interfaces [3]. Pure Al GBs [32] and Al GBs with various impurities [33, 34] have been also dealt with. The behaviour of interfacial atoms and impurities in the tensile process clearly represents the nature of interfacial bonding. We can understand the effects of impurities at GBs on the tensile behaviour from the behaviour of valence electrons or atomic bonding, which are quite important in the development of practical engineering materials.

Figure 4 shows results of the first-principles tensile test of the $\Sigma=9$ tilt GB (glide model) in Al. The tensile strength of 8.32 GPa is a little smaller than the value of 9.50 GPa obtained in [32]. This is because of the usage of GGA as the exchange-correlation functional in the present test, compared to LDA (local density approximation) used in [32]. During the tensile test, the cell sizes along the interface are fixed for simplicity, which induces additional tensile stresses parallel to the interface as σ_{22} and σ_{33} in Fig. 4. The bond-length change during the tensile test indicates enough strength of the reconstructed interfacial bonds formed by interfacial less-coordinated atoms shown in Fig. 1. In the early stage of the tensile test, we can see that the stretching of the reconstructed bonds is similar to the bulk bonds, resulting in rather high strength of this GB (over 80% of the bulk ideal strength). However, the failure initiates at these interfacial bonds due to a lower value of possible bond stretching, just after the strain of 14% corresponding to the maximum point of σ_{11} in Fig. 4.

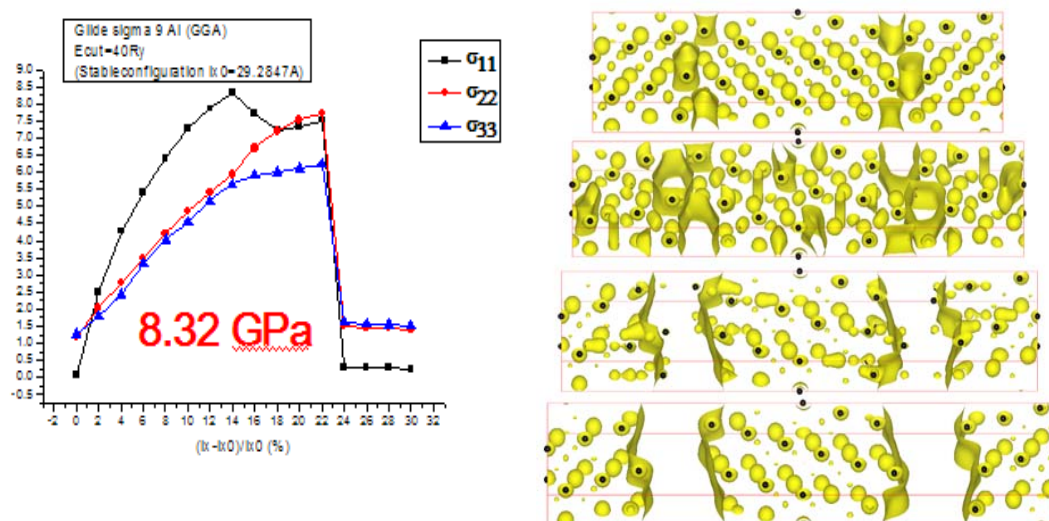


Figure 4. Results of the first-principles tensile test of the $\Sigma=9$ tilt GB (glide model) in Al. The stress-strain curve (left panel) and the evolution of atomic structure and electron distribution (charge-density iso-surfaces) during the tensile test (right panel).

Figure 5 also shows results of the first-principles tensile test of the $\Sigma=5$ twist GB in Al. The interfacial reconstruction leads to rather large tensile strength of 9 GPa. Due to the covalent nature of Al bonding, the process of tensile deformation and failure is rather complicated. Initially, the interlayer distances between the interface layer and the back layer on both sides of the interface are

enlarged due to the strength of the interfacial reconstructed bonds, which results in final complicated cleavage surfaces with two atoms per CSL unit cell previously belonging to the lower and upper crystals transferred into the upper and lower crystals, respectively, after the cleavage.

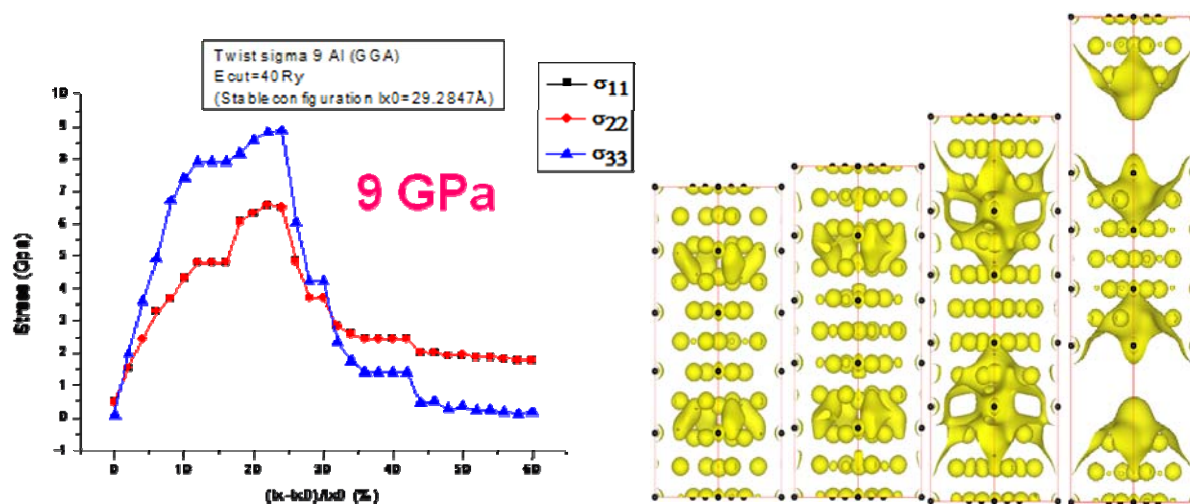
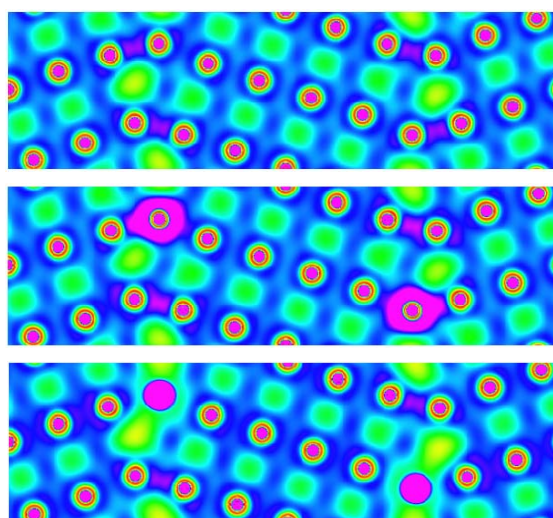


Figure 5. Results of the first-principles tensile test of the $\Sigma=5$ twist GB in Al. The stress-strain curve (left panel) and the evolution of atomic structure and electron distribution (charge-density iso-surfaces) during the tensile test (right panel).

Finally, we have examined the effects of Si and Mg impurities in the tensile behaviour of Al GBs. A recent experiment of the mechanical properties of Al micro-crystalline samples with Si, Mg and Ag impurities formed by accumulative roll bonding (ARB) has revealed quite different effects of each impurity species [7]. Both Si and Mg impurities have similar effects in decreasing grain sizes by the ARB process, resulting in similar high strength of final samples. However, the elongation until the failure for the sample containing Si is twice of that containing Mg. In other words, the Mg-impurity system cannot sustain enough plastic deformation.

Figure 6. Atomic and electronic structures of the $\Sigma=9$ tilt GB (glide model) in Al with and without segregated impurities. Pure GB (top), Si impurity (middle), and Mg impurity (bottom). Impurity atoms are located on one of four symmetric sites of less-coordinated interfacial atoms of one CSL period of the interface. Atomic relaxation was performed for the impurity systems without changing the cell sizes. Contours of valence electron density are plotted with rainbow colours. From purple of the highest density, the order of dark blue, blue, green, yellow and red corresponds to the gradual decrease in the density.



In order to elucidate the mechanism of this phenomenon, we have dealt with the models of the $\Sigma=9$ tilt GB (glide model) in Al containing substituted impurity atoms at the sites of less-coordinated atoms as shown in Fig. 6. In the pure GB, we can see the increased charge density in purple at the

interfacial reconstructed bonds. In the GB with Si, we can see the formation of strong covalent Si-Al bonds at the interface. However, in the GB with Mg, the interfacial bonding seems to be greatly weakened due to significant reduction of valence electron density between Mg and Al atoms. Figure 7 shows results of the first-principles tensile tests. As expected, the interface is greatly strengthened in the Si-impurity system, resulting in no break of the Si-Al bonds and the deformation of bulk Al regions. In the Mg-impurity system, the failure occurs at the weakened interface with lower electron density. From the present results, the shorter elongation of the Mg-impurity system in the experiment can be explained by easy initiation of failure from weakened GBs, while strengthened GBs in the Si-impurity system can maintain the plastic deformation.

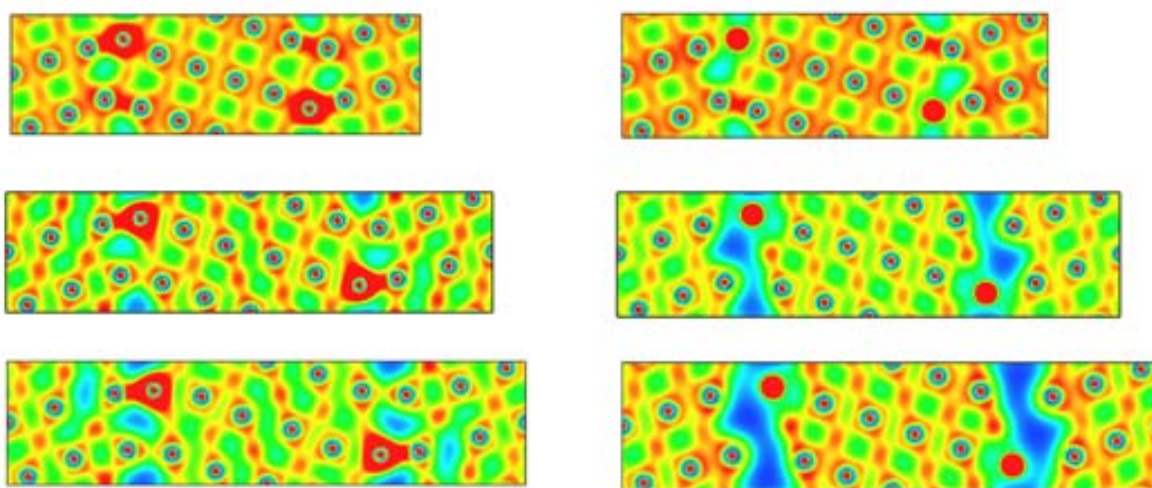


Figure 7. Evolution of the atomic and electronic structure in the first-principles tensile tests of the $\Sigma=9$ tilt GB (glide model) in Al with Si (left panel) and Mg (right panel) impurities. Contours of valence electron density are plotted by colours, where the order of red, yellow, green, blue and dark blue indicates the gradual decrease (not the same with the colours in Fig. 6).

6. Conclusion

First-principles calculations are effective tools to investigate the bonding and mechanical properties of metallic GBs. The behaviour of GBs, defects or impurities are dominated by the behaviour of valence electrons. It is important to combine first-principles calculations with experimental studies and semi-empirical large-scale simulations.

Acknowledgement

The present study was supported by Grant-in-Aid for Scientific Research (KAKENHI) on Priority Areas (No. 18062007).

References

- [1] Z. Horita, K. Ohashi, T. Fujita, K. Kaneko and T.G. Langdon, *Adv. Mater.* **17** (2005) 1599.
- [2] X. Huang, N. Hansen and N. Tsuji, *Science* **312** (2006) 249.
- [3] S. Ogata, Y. Umeno and M. Kohyama, *Model. Simul. Mater. Sci. Eng.* **17** (2009) 013001.
- [4] Y. Shiihara, M. Kohyama and S. Ishibashi, *Phys. Rev. B* **81** (2010) 075441.
- [5] S. Ishibashi, T. Tamura, S. Tanaka, M. Kohyama and K. Terakura, unpublished; <http://www.qmas.jp>
- [6] R.Z. Wang, M. Kohyama, S. Tanaka, T. Tamura and S. Ishibashi, *Mater. Trans.* **50** (2009) 11.

- [7] D. Terada, T. Masui, N. Kamikawa and N. Tsuji, *Mater. Sci. Forum* **584-586** (2008) 547.
- [8] P. E. Blöchl, *Phys. Rev. B* **50** (1994) 17953; G. Kresse and D. Joubert, *Phys. Rev. B* **59** (1999) 1758.
- [9] J. P. Perdew, K. Burke, and M. Ernzerhof, *Phys. Rev. Lett.* **77** (1996) 3865.
- [10] D. Singh, *Phys. Rev. B* **40** (1989) 5428.
- [11] N. Kosugi, *J. Comp. Phys.* **55** (1984) 426.
- [12] G.P. Kerker, *Phys. Rev. B* **23** (1981) 3082.
- [13] P. Pulay, *J. Comp. Chem.* **3** (1982) 556.
- [14] T. Tamura, G.-H. Lu, R. Yamamoto, M. Kohyama, S. Tanaka and Y. Tateizumi, *Modell. Simul. Mater. Sci. Eng.* **12** (2004) 945.
- [15] H.J. Monkhorst and J.D. Pack, *Phys. Rev. B* **13** (1976) 5188.
- [16] A.P. Sutton and R.W. Balluffi, *Interfaces in Crystalline Materials* (Oxford, 1995).
- [17] D.A. Muller and M.J. Mills, *Mater. Sci. Eng. A* **260** (1999) 12.
- [18] J.P. Hirth and J. Lothe, *Theory of Dislocations* (Wiley, New York, 2nd ed., 1982).
- [19] S. Ogata, J. Li and S. Yip, *Science* **298** (2002) 807.
- [20] C. Brandl, P.M. Derlet and H. Van Swygenhoven, *Phys. Rev. B* **76** (2007) 054124.
- [21] A.K. McMahan and J.A. Moriarty, *Phys. Rev. B* **27** (1983) 3235.
- [22] A.F. Wright and S.R. Atlas, *Phys. Rev. B* **50** (1994) 15248.
- [23] P. Ballo, J. Degmova, and V. Slugen, *Phys. Rev. B* **72** (2005) 064118.
- [24] Y. Inoue, T. Uesugi, Y. Takigawa and K. Higashi, *Mater. Sci. Forum* **561-565** (2007) 1837.
- [25] J.L.F. Da Silva, C. Barreateau, K. Schroeder and S. Blügel, *Phys. Rev. B* **73** (2006) 125402.
- [26] P.J. Feibelman, *Phys. Rev. Lett.* **65** (1990) 729.
- [27] T. Uesugi, M. Kohyama and K. Higashi, *Phys. Rev. B* **68** (2003) 184103.
- [28] O.H. Nielsen and R.M. Martin, *Phys. Rev. B* **32** (1985) 3780; 3792.
- [29] N. Chetty and R. M. Martin, *Phys. Rev. B* **45** (1992) 6074.
- [30] A. Filippetti and V. Fiorentini, *Phys. Rev. B* **61** (2000) 8433.
- [31] M. Kohyama, *Phys. Rev. B* **65** (2002) 184107.
- [32] G.-H. Lu, S. Deng, T. Wang, M. Kohyama and R. Yamamoto, *Phys. Rev. B* **69** (2004) 134106.
- [33] G.-H. Lu, Y. Zhang, S. Deng, T. Wang, M. Kohyama, R. Yamamoto, F. Liu, K. Horikawa and M. Kanno, *Phys. Rev. B* **73** (2006) 224115.
- [34] Y. Zhang, G.-H. Lu, S. Deng, T. Wang, H. Xu, M. Kohyama and R. Yamamoto, *Phys. Rev. B* **75** (2007) 174101.